Characterization of 300 GHz Wireless Channels for Rack-to-Rack Communications in Data Centers

Chia-Lin Cheng, *Student Member, IEEE* and Alenka Zajić, *Senior Member, IEEE*
Georgia Institute of Technology, Atlanta, GA 30332 USA

***Abstract*— This paper presents characterization of 300 GHz channel with optical lenses for wireless rack-to-rack data center communications. Measurements are conducted in line-of-sight (LoS), obstructed-LoS (OLoS), reflected-non-LoS (RNLoS), and obstructed-RNLoS (ORNLoS) scenarios, which evaluate the impact of obstructions such as cables on THz propagation as well as possibility of using existing metal objects as reflectors that guide waves for non-LoS type of links that are prevalent in data centers. Since optical lenses are needed to extend the communication range beyond 1m, we have evaluated path loss in such an environment and estimated path loss model parameters. The results indicate that optical lenses create a waveguide-like environment with PLEs of 1.54 in the LoS link and 1.36 in the RNLoS link. Multiple reflections are observed in PDPs when lenses are used to extend the distance but they decay as the distance increases. Additionally, reflector in the RNLoS link preserves multiple reflections longer than traditional LoS link and thus limit the coherence bandwidth B_c. Finally, when obstructions are present, the ORNLoS link has lower pathloss at distance beyond 130 cm and has less multipath compared to the OLoS link. If obstructions caused by cables are unavoidable, ORNLoS link performs better than OLoS link.**

I. Introduction

Data centers have become a critical component of cloud computing and storage [1], [2]. A fundamental need inside the data centers is reliable and high-speed connectivity between racks and blades in a data center [3]. Both metal wires and optical waveguides have been traditionally used in data centers, but they are increasing assembly cost, maintenance cost, operating cost, service time, cooling efficiency, etc. [1]–[11]. According to [12], cabling cost may take up to 3–8 % of the overall infrastructure budget. Cable bundles between server racks can lead to airflow blockages which may cause increased power consumption for cooling or failure of computers [13], [14].

One possible solution for data center rack-to-rack links is to use wireless communications. This solution will not only alleviate cable management, serviceability, and packaging constraints, but also reduce latency by providing direct communication [1]–[3], [5]–[11], [15], [16], e.g., from one rack to the rack in the next isle, as opposed to the traditional approach of routing cables above racks or down to the floor where they are connected to a router/switch. A key challenge for wireless communication in data centers is that the required data rates in existing systems are already in the hundreds of gigabits per second [17]. Terahertz (THz) wireless communication has several key advantages that can be combined to achieve the required data rates and to facilitate wireless data centers [3], [10], [11], [18]: sufficient available bandwidth around the carrier frequency—an IEEE 802.13.3d standard for THz communications proposes a data rate up to 100 Gbit/s at 252–325 GHz with 73 GHz bandwidth. Smaller antennas and antenna spacing at THz frequencies provide more multiple-input multiple-output (MIMO) antennas/channels within the same array aperture to reach Tbits/s data rates. Directionality of propagation at THz frequencies results in reduced interference and increased isolation. Furthermore, data centers provide controllable environmental conditions such as a low moisture atmosphere and limited channel mobility, which can be favorable for THz wave propagation. To develop THz communication systems, THz propagation needs to be characterized in a data center environment. While stochastic channel models for THz wireless data centers have been reported in [10], [11], [19], no channel measurements for THz rack-to-rack communications in data centers have been reported.

This paper presents characterization of 300 GHz channel with optical lenses for wireless rack-to-rack data center communications. We have performed measurements in four different wireless data center scenarios: 1) line-of-sight (LoS), 2) obstructed-LoS (OLoS), where the EM waves travel through clusters of cables, 3) reflected-non-LoS (RNLoS) link, where a metal reflector is used to guide signals in desired direction, 4) obstructed-RNLoS (ORNLoS) with obstruction of cables placed between the T_{x}/R_{x} and the reflector. We investigate these four scenarios to evaluate the impact of obstructions such as cables on THz propagation as well as possibility of using existing metal objects as reflectors that guide signals for non-LoS type of links that are prevalent in data centers.

We start by analyzing path loss in a rack-to-rack data center environment. Results indicate that optical lenses create a waveguide-like environment with path loss exponents (PLEs) of 1.54 in the LoS link and 1.36 in the RNLoS link. Multiple reflections are observed in power delay profiles (PDPs) when lenses are used to extend the distance. Additionally, reflector in the RNLoS link preserves multiple reflections longer than traditional LoS link and thus limits the coherence bandwidth B_c and the maximum data rate. Furthermore, the optimal LoS T_{x}–R_{x} separation distance that results in the widest B_c (around 7 GHz) is identified at distances between 180–210 cm. Finally, when obstructions are present, the ORNLoS environment experiences about 5 dB less loss at distances

This work has been supported, in part, by NSF grant 1651273. The views and findings in this paper are those of the authors and do not necessarily reflect the views of NSF.

larger than 130 cm and experiences less multipath as compared to the OLoS link. This result indicates that ORNLoS scenario might be a good way to set up wireless communication links in data centers.

The remainder of this paper is organized as follows. Section II introduces the THz equipment and the PTFE lens configuration. Section III describes four measurement scenarios. Section IV presents measurement results and analysis for each scenario. Finally, Section V provides some concluding remarks.

II. Measurement Setup

The measurement setup consists of the N5224A PNA vector network analyzer (VNA), the VDI transmitter (Tx210) and the VDI receiver (Rx148) [20]. The T_{x} output power is around -15 dBm. The antenna used in the measurement is a vertically polarized pyramidal horn with gain that varies from 22 to 24 dBi from 300 GHz to 320 GHz. The theoretical half-power beamwidth (HPBW) is about 10° in azimuth and elevation. Detailed measurement parameters and instrument description can be found in [17].

Two plano-convex Polytetrafluoroethylene (PTFE/Teflon) lenses with a focal length of 7.5 cm and a diameter of 5 cm are used to collimate the THz beam and provide extra gain. The relative position of lenses and T_{x}/R_{x} are shown in Fig. 1. Note that when changing the T_{x}–R_{x} distance, the distance between horns and lenses is fixed at 6 cm. Only the distance between two lenses (d') varies. The horn–lens distance of 6 cm is slightly different than the focal length of 7.5 cm since it needs to be fine-tuned regarding the operating frequency.

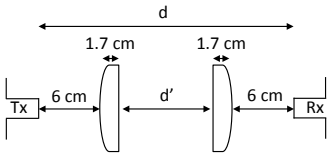

Fig. 1. Plano-convex PTFE lens configuration.

III. Measurement Scenarios

In this measurement campaign, four rack-to-rack wireless data center scenarios have been considered: 1) LoS, 2) OLoS, 3) RNLoS, and 4) ORNLoS.

A. LoS Link

In rack-to-rack scenario [5], transceivers are mounted on top of the server racks to enable wireless links between racks. Our measurement setup for LoS link is presented in Fig. 2 (a). We place THz T_{x}/R_{x} and lens on top of two separate metal cabinets, where the metal cabinets act as server racks in a data center. The THz beam with optical lenses is focused to ensure that no reflection from ground, metal cabinets (both hollow and solid sides), or any other objects outside the lens diameter is present in the wireless channel. The LoS measurements have been recorded as the horn-to-horn distance d is varied from 40 cm to 210 cm in 5 cm increments, where the maximum distance is limited by the synchronization cable used between the T_{x} and R_{x}. Note that we have verified that no reflections from the ground or any neighboring objects are present in the signal.

B. OLoS Link

Here we consider a scenario where the wireless channel is obstructed by cables, which is one of the most common objects in data centers. The measurement setup for OLoS link is presented in Figs. 2 (b) and (c). Based on the same setup in Section III-A, we obstruct the LoS channel with a cluster of cables, which are hung in the air by a tripod. By using a tripod to hold cables, we can make sure cables are fixed at the same position while T_{x}/R_{x} are moving. The OLoS measurements have been recorded at d=40 cm–210 cm in 10 cm increments.

C. RNLoS Link

RNLoS links are presented to improve the transmission range and concurrent number of wireless links and allow transceivers to bypass obstacles to communicate directly without multi-hop relays [5]. Most RNLoS links in mm-wave wireless data centers [2], [5]–[7], [11] use the entire ceiling in a server room as reflectors, which takes huge space and increases cost. Our measurement setup in Fig. 2 (d) demonstrates that to enable a RNLoS link in a THz wireless data center, a palm-sized compact reflector would be sufficient due to extremely focused THz beam. Note that the geometry of the reflector needs to accommodate the size of the lens. We design an aluminum square-shape reflector with a side length of 15 cm, which is roughly twice the lens diameter. The RNLoS measurements have been recorded at d=40 cm–210 cm in 5 cm increments.

D. ORNLoS Link

Our measurement setup for ORNLoS link is presented in Figs. 2 (e) and (f). Similar to the setup in Section III-C, here we place the tripod with obstructing cables between the T_{x} and the reflector. The ORNLoS measurements have been recorded at d=40 cm–210 cm in 10 cm increments.

IV. Measurement Results and Analysis

A. Path Loss and Multipath Characterization

In this paper, the mean of measured path loss, $\overline{PL}$, is obtained by averaging a swept continuous wave over time and frequency, i.e.,

$$\overline{PL(d)} = \frac{1}{MN}\sum_{i=1}^{N}\sum_{j=1}^{M}|H(f_i,t_j,d)|^2, \tag{1}$$

where $H(f_i,t_j,d)$ is the measured complex frequency response data, M is the number of frequency-response snapshots over time, N is the number of observed frequencies, and d is the T_{x}–R_{x} horn-to-horn separation distance. We model the mean path loss by the single-frequency floating-intercept (FI, alpha-beta, or the 3rd Generation Partnership Project 3GPP) model due to better susceptibility to measurement errors [21]. The FI path loss model is given as follows [22, pp. 16–21]:

$$PL^{FI}(d) = \alpha + 10\beta\log_{10}\left(\frac{d}{d_0}\right) + X_{\sigma}^{\mathrm{FI}}, d \geq d_0, \tag{2}$$

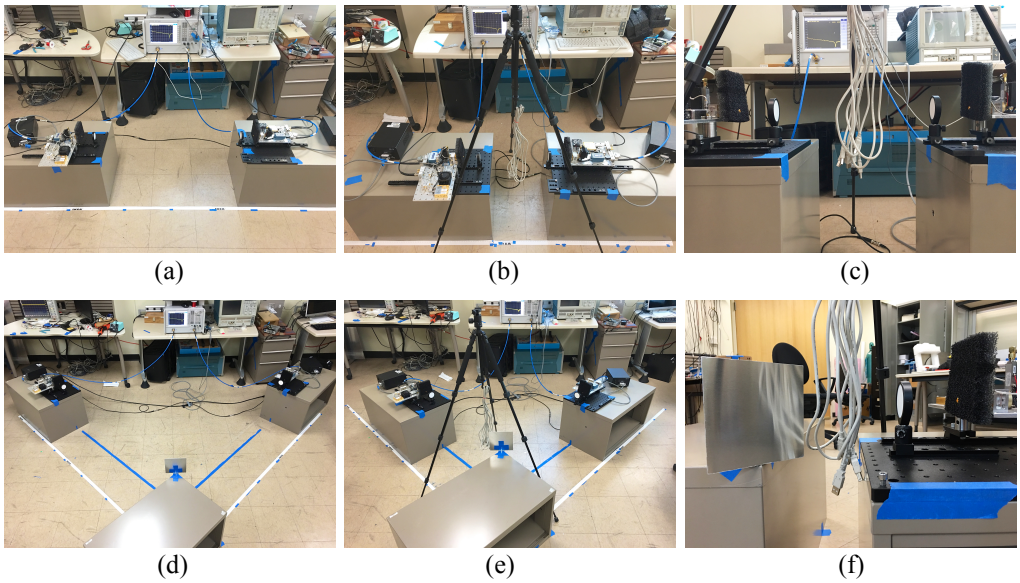

Fig. 2. Measurement scenarios: (a) LoS, (b)/(c) OLoS with cables as obstruction, (d) RNLoS, (e)/(f) ORNLoS with cables as obstruction.

where $PL_{FI}(d)$ is the path loss in dB as a function of d, α is a floating intercept in dB that represents the free-space path loss at the reference distance d_0 = 20 cm, β is the PLE that characterizes the dependence of path loss on d, and X_{σ}^{FI} is the large-scale shadow fading that can be modeled as a zero-mean Gaussian distributed random variable with standard deviation σ in dB. To estimate the path loss model parameters α, β, and σ, the least-squares linear fitting is performed through the measured path loss data sets such that the root mean square (rms) deviation from the mean path loss is minimized.

The channel impulse response is obtained by taking the inverse discrete Fourier transform (IDFT) of the measured channel frequency response. Root-mean-square (rms) delay spread calculated by taking the square root of the second central moment of the normalized squared magnitude of the channel impulse response, i.e.,

$$\tau_{rms} = \sqrt{\sum_{k=1}^{L}(\tau_k - \tau_m)^2 |h(t,\tau_k,d)|^2}, \tag{3}$$

where L is the number of multipath components, τ_k is the excess delay of the k^{th} path relative to the first arrival, and τ_m is the mean excess delay defined as

$$\tau_m = \sum_{k=1}^{L} \tau_k \cdot |h(t,\tau_k,d)|^2. \tag{4}$$

The coherence bandwidth (B_c) is calculated as [22],

$$B_c = 1/2 \cdot \pi \cdot \tau_{rms}. \tag{5}$$

B. Characterization of LoS and RNLoS Links

In this section, we investigate the measured path loss and the relationship between T_{x}–R_{x} distance and the corresponding path loss, PDPs, and B_c in the LoS and RNLoS scenarios shown in Figs. 2 (a)–(c).

For the path loss measurements, Figs. 3 (a) and (b) present the measured path loss with T_{x}–R_{x} distances varying from 50 cm to 210 cm in LoS and RNLoS scenarios, respectively. Periodic ripples in path loss curves are the strongest for the short distances and gradually attenuate as distance increases. This is because the periodic ripples are caused by multiple reflections between lenses and horns that gradually decay as the distance increases. Note that the periodic path loss ripples with peak-to-peak values up to 4 dB are not caused by the antenna gain diagram since the peak-to-peak antenna gain variations over frequency are only around 0.6 dB. Compared to the path loss measured in free space without using lenses [21], here we can observe that path loss curves have less fluctuations with frequency and that signal experiences less loss. We can also observe that LoS and RNLoS links have similar path loss values that range between 50 dB–65 dB for distances between 50 cm–210 cm and that the RNLoS link has more congested path loss curves as the distance increases.

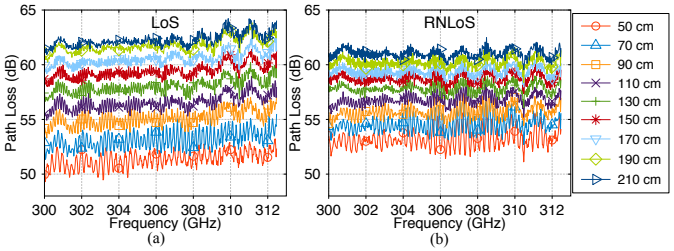

Fig. 3. Measured path loss curves in (a) LoS and (b) RNLoS scenarios at d=50, 70, 90, 110, 130, 150, 170, 190, 210 cm.

For the comparison of path loss models, Fig. 4 presents the measured mean path loss and the FI path loss models for the LoS and RNLoS scenarios at d=40 cm–210 cm. For the LoS path loss model, the PLE is β=1.54, the path loss at the reference distance of 20 cm is α=45.2 dB, and the standard deviation is σ=0.6 dB. For the RNLoS path loss model, the PLE is β=1.36, the path loss at the reference distance of 20 cm is α=47.2 dB, and the standard deviation is σ=0.4 dB. It is observed that the RNLoS path loss model has a lower PLE, which coincides with the observation of more congested

path loss curves in Fig. 3 (b). Results show that optical lenses create a waveguide-like environment, resulting in PLEs less than 2.

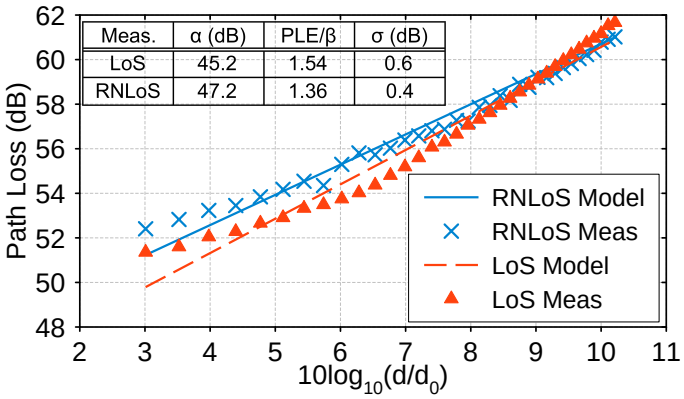

Fig. 4. Measured mean path loss and FI path loss models for LoS and RNLoS scenarios at d=40 cm–210 cm.

Figure 5 shows the measured PDPs for LoS and RNLoS scenarios at distances between 50 cm and 210 cm. Distinctive multipaths can be categorized into three clusters labeled as 1, 2, and 3 in Fig. 5. Cluster 1 results from reflections between (T_x lens and T_x horn) and (R_x lens and R_x horn). Note that cluster 1 does not move as distance increases since the lens–horn distance is fixed at 6 cm as shown in Fig. 1. Cluster 2 is a combination of reflections between T_x lens and R_x lens (path d' in Fig. 1) and reflections between R_x lens and R_x horn. Cluster 3 is due to R_x horn-to-T_x horn reflection. Note that since the surrounding area of T_x and R_x horns are covered with absorbers, the horn-related multiple reflections come from the tips and internal surfaces of the horns. In Figs. 5 (a) and (b), it is observed that both LoS and RNLoS links have similar PDPs distribution at d=50 cm–110 cm. As distance increases to 110 cm–180 cm, clusters 2 and 3 in the LoS link and cluster 3 in the RNLoS link gradually decay below PDP threshold (cluster 3 decays at a faster rate than cluster 2), while cluster 2 in the RNLoS link still remains observable. As distance increases to 185 cm–210 cm, only cluster 1 in the LoS link remains as shown in Fig. 5 (a). In contrast, both clusters 1 and 2 in the RNLoS link remain observable at distance up to 210 cm as shown in Fig. 5 (b) at around 12–14 ns. The comparison in Figs. 5 (a) and (b) shows that the reflector in RNLoS link preserves reflections between T_x lens and R_x lens and sustains cluster 2 in PDPs across distances of 50 cm–210 cm. This difference in PDPs between LoS and RNLoS links affects B_c and the maximum data rate.

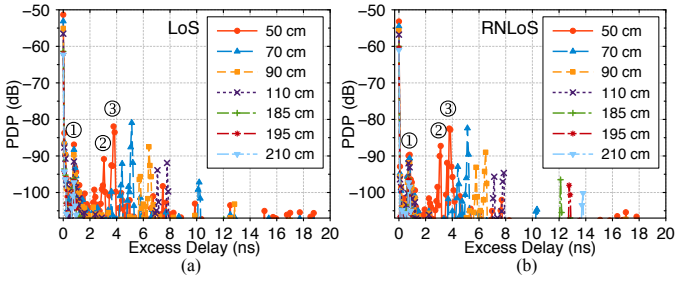

Fig. 5. Measured PDPs for (a) LoS and (b) RNLoS scenarios at d=50, 70, 90, 110, 185, 195, 210 cm.

Figure 6 shows the measured B_c for LoS and RNLoS scenarios at d=40–210 cm. In the RNLoS link, B_c stays between 1-2 GHz across all distances due to constant existence of PDP cluster 2, while in the LoS link, B_c increases to 7 GHz at distances between 180 cm–210 cm since the PDP cluster 2 eventually attenuates below PDP threshold. Limited B_c in the RNLoS link limits the maximum data rate.

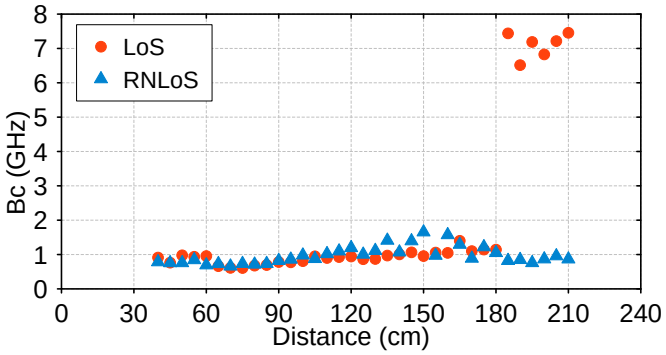

Fig. 6. Measured B_c for LoS and RNLoS scenarios at d=40–210 cm.

C. Characterization of OLoS and ORNLoS Links

In this section, we study the measured path loss and the relationship between T_x–R_x distance and the corresponding path loss, PDPs, and B_c in the OLoS and ORNLoS links with cables as obstruction shown in Figs. 2 (d)–(f).

Figures 7 (a) and (b) compare the measured path loss in OLoS and ORNLoS links at d=50, 110, 150, 210 cm. It is observed that the ORNLoS link achieves lower path loss (5 dB lower at distances beyond 130 cm) and less path loss fluctuations with frequency as compared to the OLoS link. Since the curvature of cables are comparable to the wavelength at 300 GHz, the wave experiences a combination of reflection and diffraction when propagating through cables; the reflector in ORNLoS link helps to "collect" these reflected waves and transmit them from the T_x to the R_x and thus leads to lower path loss as compared to the OLoS link.

Figures 8 (a) and (b) show the measured PDPs for OLoS and ORNLoS links at d=50, 110, 150, 210 cm. It is observed that the most of the dominant multipath clusters (cluster 2 and 3) in Figs. 5 (a) and (b) are no longer observable in the presence of obstructing cables.

Figure 9 shows the measured B_c for OLoS and ORNLoS scenarios at d=40–210 cm. It is observed that as distance increases from 40 cm to 210 cm, B_c drops from around 1 GHz to around 0.2 GHz. The ORNLoS link has a wider B_c than the OLoS link by around 0.2 GHz across distances, which is a result of ORNLoS link's suppressed multipath.

V. Conclusions

This paper presents characterization of 300 GHz channel for wireless rack-to-rack data center communications. Measurements are conducted in LoS, OLoS, RNLoS, and ORNLoS scenarios to evaluate the impact of obstructions such as cables on THz propagation as well as possibility of using existing metal objects as reflectors to guide signals in non-LoS type of links. Since optical lenses are needed to extend

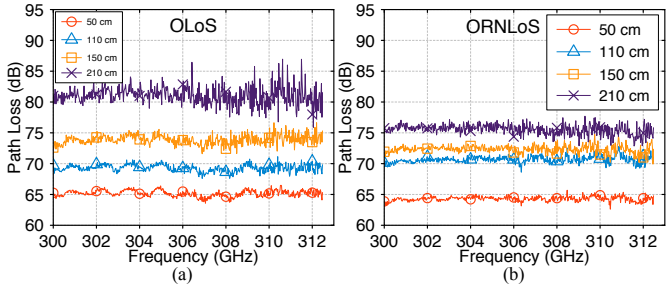

Fig. 7. Measured path loss curves in (a) OLoS and (b) ORNLoS scenarios at d=50, 110, 150, 210 cm.

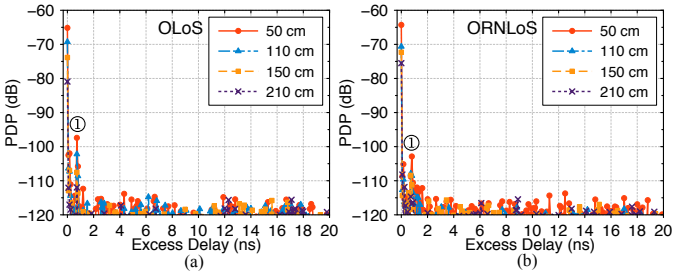

Fig. 8. Measured PDPs for (a) OLoS and (b) ORNLoS scenarios at d=50, 110, 150, 210 cm.

the communication range beyond 1m, we have evaluated path loss in such an environment and estimated path loss model parameters. The results indicate that optical lenses create a waveguide-like environment with PLEs of 1.54 in the LoS link and 1.36 in the RNLoS link. Multiple reflections are observed in PDPs when lenses are used to extend the distance. Additionally, reflector in the RNLoS link preserves multiple reflections longer than traditional LoS link and thus limit the coherence bandwidth. Finally, when obstructions are present, the ORNLoS link has lower pathloss at distance beyond 130 cm and has less multipath compared to the OLoS link. If obstructions caused by cables are unavoidable, ORNLoS link performs better than OLoS link.

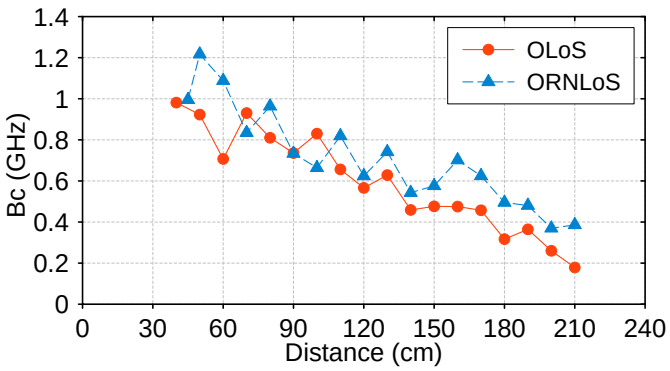

Fig. 9. Measured B_c for OLoS and ORNLoS scenarios at d=40–210 cm.

References

[1] Y. Cui, H. Wang, X. Cheng, and B. Chen, "Wireless data center networking," *IEEE Wireless Communications*, vol. 18, no. 6, pp. 46–53, December 2011.

[2] C. Zhang, F. Wu, X. Gao, and G. Chen, "Free talk in the air: A hierarchical topology for 60 ghz wireless data center networks," *IEEE/ACM Transactions on Networking*, vol. 25, no. 6, pp. 3723–3737, Dec 2017.

[3] K. Ramachandran, R. Kokku, R. Mahindra, and S. Rangarajan, "60 ghz data-center networking: Wireless = worry less?" in *NEC Technical Report*, 2008.

[4] G. Chen, H. Chen, M. Haurylau, N. A. Nelson, D. H. Albonesi, P. M. Fauchet, and E. G. Friedman, "On-chip copper-based vs. optical interconnects: Delay uncertainty, latency, power, and bandwidth density comparative predictions," in *2006 International Interconnect Technology Conference*, June 2006, pp. 39–41.

[5] T. Chen, X. Gao, and G. Chen, "The features, hardware, and architectures of data center networks: A survey," *Journal of Parallel and Distributed Computing*, vol. 96, pp. 45 – 74, 2016.

[6] W. Zhang, X. Zhou, L. Yang, Z. Zhang, B. Y. Zhao, and H. Zheng, "3d beamforming for wireless data centers," in *Proceedings of the 10th ACM Workshop on Hot Topics in Networks*, ser. HotNets-X. New York, NY, USA: ACM, 2011, pp. 4:1–4:6.

[7] X. Zhou, Z. Zhang, Y. Zhu, Y. Li, S. Kumar, A. Vahdat, B. Y. Zhao, and H. Zheng, "Mirror mirror on the ceiling: Flexible wireless links for data centers," in *Proceedings of the ACM SIGCOMM 2012 Conference on Applications, Technologies, Architectures, and Protocols for Computer Communication*, ser. SIGCOMM '12. New York, NY, USA: ACM, 2012, pp. 443–454.

[8] D. Halperin, S. Kandula, J. Padhye, P. Bahl, and D. Wetherall, "Augmenting data center networks with multi-gigabit wireless links," *SIGCOMM Comput. Commun. Rev.*, vol. 41, no. 4, pp. 38–49, Aug. 2011.

[9] J. Y. Shin, E. G. Sirer, H. Weatherspoon, and D. Kirovski, "On the feasibility of completely wireless datacenters," in *2012 ACM/IEEE Symposium on Architectures for Networking and Communications Systems (ANCS)*, Oct 2012, pp. 3–14.

[10] A. Davy, L. Pessoa, C. Renaud, E. Wasige, M. Naftaly, T. Kürner, G. George, O. Cojocari, N. O. Mahony, and M. A. G. Porcel, "Building an end user focused thz based ultra high bandwidth wireless access network: The terapod approach," in *2017 9th International Congress on Ultra Modern Telecommunications and Control Systems and Workshops (ICUMT)*, Nov 2017, pp. 454–459.

[11] B. Peng and T. Kürner, "A stochastic channel model for future wireless thz data centers," in *2015 International Symposium on Wireless Communication Systems (ISWCS)*, Aug 2015, pp. 741–745.

[12] L. Popa, S. Ratnasamy, G. Iannaccone, A. Krishnamurthy, and I. Stoica, "A cost comparison of datacenter network architectures," in *Proceedings of the 6th International COnference*, ser. Co-NEXT '10. New York, NY, USA: ACM, 2010, pp. 16:1–16:12.

[13] L. A. Barroso, J. Clidaras, and U. Höelzle, *The Datacenter as a Computer: An Introduction to the Design of Warehouse-Scale Machines, Second Edition*, 2nd ed. Morgan and Claypool Publishers, 2013.

[14] Cisco. (2017) Cisco unified computing system site planning guide: Data center power and cooling. [Online]. Available: https://www.cisco.com/c/en/us/solutions/collateral/data-center-virtualization/unified-computing/white_paper_c11-680202.pdf

[15] H. Vardhan, N. Thomas, S. R. Ryu, B. Banerjee, and R. Prakash, "Wireless data center with millimeter wave network," in *2010 IEEE Global Telecommunications Conference GLOBECOM 2010*, Dec 2010, pp. 1–6.

[16] E. Baccour, S. Foufou, R. Hamila, and M. Hamdi, "A survey of wireless data center networks," in *2015 49th Annual Conference on Information Sciences and Systems (CISS)*, March 2015, pp. 1–6.

[17] S. Kim and A. Zajić, "Characterization of 300-ghz wireless channel on a computer motherboard," *IEEE Transactions on Antennas and Propagation*, vol. 64, no. 12, pp. 5411–5423, Dec 2016.

[18] IEEE, "Technical requirements document," in *IEEE 802.15-14/0309r20*, Mar 2016.

[19] V. Petrov, J. Kokkoniemi, D. Moltchanov, J. J. Lehtomäki, Y. Koucheryavy, and M. J. Juntti, "Last meter indoor terahertz wireless access: Performance insights and implementation roadmap," *CoRR*, vol. abs/1708.02963, 2017.

[20] [Online]. Available: http://vadiodes.com/en/products/custom-transmitters

[21] C. L. Cheng, S. Kim, and A. Zajić, "Comparison of path loss models for indoor 30 ghz, 140 ghz, and 300 ghz channels," in *2017 11th European Conference on Antennas and Propagation (EUCAP)*, March 2017, pp. 716–720.

[22] A. Zajić, *Mobile-to-Mobile Wireless Channels*. Norwood, MA, USA: Artech House, Inc., 2013.